Proceedings of the 2001 IEEE/RSJ
International Conference on Intelligent Robots and Systems
Maui, Hawaii, USA, Oct. 29 – Nov. 03, 2001

Optimal Architecture Design of Parallel Manipulators for Best Accuracy

Jeha Ryu* **Jongeun Cha****
Department of Mechatronics
Kwangju Institute of Science and Technology
1 Oryong-dong, Puk-gu, Kwangju 500-712, Korea
*ryu@kjist.ac.kr **gaecha@geguri.kjist.ac.kr

Abstract

This paper presents a design optimization method of parallel manipulators for best accuracy. An accurate kinematic error model that relates every structural error source in the manipulator's structure to end-effector pose errors is derived for a HexaSlide type parallel manipulator. Based on the error model, a measure of accuracy, Error Amplification Factor (*EAF*), is introduced for an optimum design formulation with constraints on workspace and design variable limits. Then, design optimization for best accuracy has been performed by using a nonlinear optimization technique. Optimization results have been validated by Monte Carlo statistical simulation technique. The optimized design shows smaller error than the initial design.

1. Introduction

Optimal kinematic design of robot manipulators is very important for achieving desired performances. Recently, optimum architecture design of parallel manipulators has drawn much attention because of advantages of higher stiffness, accuracy, payload, etc, over serial manipulators. In the optimum design, stiffness, workspace, accuracy, dexterity, isotropy, maximum working speed and payload have been used as performance criteria. Among them, dexterity has been considered important, because it is a measure of ability of a manipulator to arbitrarily change its position and orientation or to apply forces and torques in arbitrary direction. Many researchers[1-6] therefore had performed design optimization focusing on the dexterity of parallel manipulators in terms of the condition number of the Jacobian matrix. Workspace also has been taken into account for design purposes by some researchers[7-10]. Other researchers[11-14] included simultaneously dexterity, workspace, and stiffness for the design of parallel manipulators. Hong and Kim[15] proposed a new performance measure by combining the condition number with the manipulability ellipsoid volume and maximized it for rapid machining and maximum force transmission of the Eclipse.

Accuracy of a robot manipulator is also an important design criterion for very fine motion tasks such as coordinate measurement, medical operation, and micro-manipulation. Accuracy of a manipulator can be affected by many factors such as driving actuator control errors, installation errors, manufacturing tolerances and clearances, architecture design, etc. Wang and Masory[16] presented a kinematic error model for a Stewart platform using the D-H convention which takes into account manufacturing errors and investigated effects of manufacturing tolerances on the platform pose accuracy. Ropponen and Arai[17] presented, for the modified Stewart platform, the closed kinematic error model including the joint position errors and the actuation errors by differentiating the inverse kinematics equation. They then computed the error ellipsoids and the position errors of end-effector. Patel and Ehmann[18] derived a kinematic error model of the Stewart platform that accounts for all sources of errors (including such varied effects as manufacture error, thermal and stress strains, control error, etc.) and plotted error gain sensitivity. They showed that errors would be attenuated through the kinematic structure design. Bi et al[19] applied Ropponen and Arai's approach to the Serial-parallel micromotion manipulator and derived error effects that are useful for the design and manufacture of the manipulator. Xi and Mechefske[20] presented an error equation of a HexaSlide manipulator using the inverse kinematic equation and evaluated the platform pose errors applying the matrix norms. They showed that the error transmission between the moving axes and the moving platform is closely related to the condition number of the Jacobian matrix. Pasek[21] analyzed the manipulator's accuracy based on the Monte Carlo statistical experiment approach and a Jacobian approximation. The aforementioned research about the accuracy is, however, mainly for evaluating the end-effector pose errors based on a kinematic error models.

In this paper, we present a design optimization method of parallel manipulators for the best accuracy. Even though there have been many researches on the design optimization for dexterity, isotropy, load carrying capability, and workspace, there are a few researches on design optimization for accuracy. Our approach is based on an accurate error model that includes every kinematic error sources. As an example, an error analysis of a HexaSlide type parallel manipulator has been performed by using inverse kinematics model and we derived an error transformation matrix from all error sources to the end-effector pose error. Then an error amplification factor

0-7803-6612-3/01/$10.00©2001 IEEE

(EAF) is defined as a volume of error ellipsoid. The EAF is used in design optimization for best accuracy as a main performance criterion. An optimization problem is then formulated considering constraints on workspace and design variable limits. The accuracy improvement through the proposed design optimization is evaluated by the Monte Carlo simulation.

This paper is organized as follows; in section II, the geometry and nomenclature of the HexaSlide manipulator are described. Section III derives an accurate kinematic error model that includes all error sources. Also, an error transformation matrix is introduced for optimal design formulation. In section IV, an error amplification factor is defined as an accuracy criterion based on the singular value analysis of the error transformation matrix. In section V, an optimization problem is formulated for best accuracy design. In section VI, the results of the optimization and validation by Monte Carlo simulation are presented. In section VII, conclusions and discussions are given.

2. Description of the HSM

A HexaSlide manipulator (HSM) shown in Fig.1 is composed of six links, a mobile platform, and six prismatic actuators fixed to the base. The links are connected to the actuators and the platform by spherical and universal joints pair. This manipulator controls the pose of the platform by moving the spherical joints, A_i, from $A_{i,0}$ to $A_{i,1}$ with six actuators. The base coordinate frame XYZ is placed on the center O of the base. The origin of the platform coordinate frame xyz is attached to the center C of the moving platform. Note that the point C may be a tip of machining tool or a tip of the touch probe in a coordinate measuring machine. All vectors and matrices will be denoted in bold letters. A pose of the platform is expressed by a position vector **OC** and a rotation matrix **R**;

$$\mathbf{OC}=[X_C \quad Y_C \quad Z_C] \qquad \mathbf{R}=\mathbf{R}_{X,\theta}\mathbf{R}_{Y,\psi}\mathbf{R}_{z,\phi} \tag{1}$$

3. Volumetric Error Analysis

Errors in the kinematic structure, such as manufacturing tolerances and clearances, installation errors, and control errors, lead to the pose errors of the mobile platform. In this section, a relationship between the structural errors and the pose errors is discussed.

Fig. 2 shows the i-th chain and kinematic parameters of the HSM. In this figure, vectors $\mathbf{a}_i$ and $\mathbf{n}_i$ are the unit vectors along the actuation and link direction respectively, and λ_i is an articular variable that is the distance between $A_{i,0}$ and A_i points. A closed-loop vector equation of the i-th chain is given by

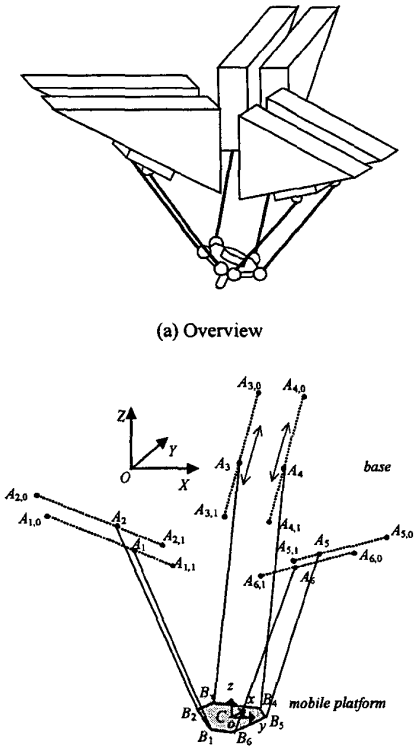

(a) Overview

(b) Schematic Diagram

Fig. 1. HexaSlide Parallel Manipulator

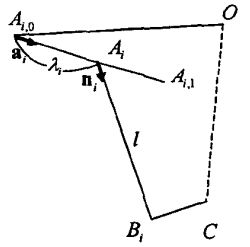

Fig. 2. Schematic Diagram of One Chain

$$\lambda_i\mathbf{a}_i=\mathbf{OC}+\mathbf{RCB}_i'-\mathbf{OA}_{i,0}-l_i\mathbf{n}_i \tag{2}$$

where $\mathbf{CB}_i'$ vector is represented in the platform coordinate frame.

A differential error model is obtained by differentiating Eq.(2) as

$$\delta\lambda_i\mathbf{a}_i+\lambda_i\delta\mathbf{a}_i=\delta\mathbf{OC}+\delta\mathbf{RCB}_i'+\mathbf{R}\delta\mathbf{CB}_i'-\delta\mathbf{OA}_{i,0}-l_i\delta\mathbf{n}_i-\delta l_i\mathbf{n}_i \tag{3}$$

where the derivative of the rotation matrix is given by

$$\delta\mathbf{R} = \delta\tilde{\boldsymbol{\theta}}\mathbf{R} = \begin{bmatrix} 0 & -\delta\theta_z & \delta\theta_y \\ \delta\theta_z & 0 & -\delta\theta_x \\ -\delta\theta_y & \delta\theta_x & 0 \end{bmatrix}\mathbf{R} \tag{4}$$

Using Eq.(4), Eq.(3) can be rewritten as

$$\begin{aligned}\delta\lambda_i\mathbf{a}_i + \lambda_i\delta\mathbf{a}_i &= \delta\mathbf{OC} + \delta\tilde{\boldsymbol{\theta}}\mathbf{RCB}_i' + \mathbf{R}\delta\mathbf{CB}_i' - \delta\mathbf{OA}_{i,0} - l_i\delta\mathbf{n}_i - \delta l_i\mathbf{n}_i \\ &= \delta\mathbf{OC} + \delta\boldsymbol{\theta}\times\mathbf{CB}_i + \mathbf{R}\delta\mathbf{CB}_i' - \delta\mathbf{OA}_{i,0} - l_i\delta\mathbf{n}_i - \delta l_i\mathbf{n}_i\end{aligned} \tag{5}$$

Multiplication of $\mathbf{n}_i^T$ on both sides of Eq.(5) gives

$$\mathbf{n}_i^T\mathbf{a}_i\delta\lambda_i = \mathbf{n}_i^T\delta\mathbf{OC} + (\mathbf{n}_i\times\mathbf{B}_i\mathbf{C})^T\delta\boldsymbol{\theta} + \mathbf{n}_i^T\mathbf{R}\delta\mathbf{CB}' - \mathbf{n}_i^T\delta\mathbf{OA}_{i,0} - \delta l_i - \mathbf{n}_i^T(\lambda_i\delta\mathbf{a}_i) \tag{6}$$

since $\mathbf{n}_i^T\mathbf{n}_i = 1$ and $\mathbf{n}_i^T\delta\mathbf{n}_i = 0$. Considering all 6 links, Eq.(6) can be combined into a matrix form as

$$\mathbf{J}^{-1}\delta\mathbf{X} = \delta\boldsymbol{\Lambda} + \mathbf{M}\delta\mathbf{L} + \mathbf{N}_1\delta\mathbf{CB}' + \mathbf{N}_2(\delta\mathbf{OA}_0 + \delta\mathbf{A}) \tag{7}$$

where

$$\delta\mathbf{X} = [\delta\mathbf{OC} \quad \delta\boldsymbol{\theta}]^T = [\delta X_C \quad \delta Y_C \quad \delta Z_C \quad \delta\theta_X \quad \delta\theta_Y \quad \delta\theta_Z]^T \tag{8}$$

$$\delta\boldsymbol{\Lambda} = [\delta\lambda_1 \quad \delta\lambda_2 \quad \delta\lambda_3 \quad \delta\lambda_4 \quad \delta\lambda_5 \quad \delta\lambda_6]^T \tag{9}$$

$$\delta\mathbf{L} = [\delta l_1 \quad \cdots \quad \delta l_6]^T \tag{10}$$

$$\delta\mathbf{CB}' = \begin{bmatrix} \delta\mathbf{CB}_1' \\ \vdots \\ \delta\mathbf{CB}_6' \end{bmatrix} \in \Re^{18\times 1} \qquad \delta\mathbf{OA}_0 = \begin{bmatrix} \delta\mathbf{OA}_{1,0} \\ \vdots \\ \delta\mathbf{OA}_{6,0} \end{bmatrix} \in \Re^{18\times 1} \tag{11}$$

$$\delta\mathbf{A} = \begin{bmatrix} \lambda_1\delta\mathbf{a}_1 \\ \vdots \\ \lambda_6\delta\mathbf{a}_6 \end{bmatrix} \in \Re^{18\times 1} \tag{12}$$

$$\mathbf{J}^{-1} = \begin{bmatrix} \dfrac{\mathbf{n}_1^T}{\mathbf{a}_1^T\mathbf{n}_1} & \dfrac{(\mathbf{n}_1\times\mathbf{B}_1\mathbf{C})^T}{\mathbf{a}_1^T\mathbf{n}_1} \\ \vdots & \vdots \\ \dfrac{\mathbf{n}_6^T}{\mathbf{a}_6^T\mathbf{n}_6} & \dfrac{(\mathbf{n}_6\times\mathbf{B}_6\mathbf{C})^T}{\mathbf{a}_6^T\mathbf{n}_6} \end{bmatrix} \in \Re^{6\times 6} \tag{13}$$

$$\mathbf{M} = \begin{bmatrix} \dfrac{1}{\mathbf{a}_1^T\mathbf{n}_1} & \cdots & 0 \\ \vdots & \ddots & \vdots \\ 0 & \cdots & \dfrac{1}{\mathbf{a}_6^T\mathbf{n}_6} \end{bmatrix} \in \Re^{6\times 6} \tag{14}$$

$$\mathbf{N}_1 = \begin{bmatrix} \dfrac{-\mathbf{n}_1^T\mathbf{R}}{\mathbf{a}_6^T\mathbf{n}_6} & \cdots & 0 \\ \vdots & \ddots & \vdots \\ 0 & \cdots & \dfrac{-\mathbf{n}_6^T\mathbf{R}}{\mathbf{a}_6^T\mathbf{n}_6} \end{bmatrix} \in \Re^{6\times 18} \tag{15}$$

$$\mathbf{N}_2 = \begin{bmatrix} \dfrac{\mathbf{n}_1^T}{\mathbf{a}_6^T\mathbf{n}_6} & \cdots & 0 \\ \vdots & \ddots & \vdots \\ 0 & \cdots & \dfrac{\mathbf{n}_6^T}{\mathbf{a}_6^T\mathbf{n}_6} \end{bmatrix} \in \Re^{6\times 18} \tag{16}$$

Note that $\delta\mathbf{X}$ is the platform pose error vector, $\delta\boldsymbol{\Lambda}$ is a control error vector of the actuators, $\delta\mathbf{L}$ is a length error vector of the links due to manufacturing tolerance and installation errors, $\delta\mathbf{CB}'$ and $\delta\mathbf{OA}_0$ are position error vectors of B_i and $A_{i,0}$, and $\delta\mathbf{A}$ is an alignment error vector in the actuator axis. Note also that not only the inverse Jacobian matrix $\mathbf{J}^{-1}$ but also other matrices, $\mathbf{M}$, $\mathbf{N}_1$, $\mathbf{N}_2$, which are dependent on the configuration of the manipulator, transform the errors in the kinematic structure to the errors of the platform.

If $\mathbf{J}^{-1}$ is invertible, Eq.(7) can be rewritten as

$$\delta\mathbf{X} = \mathbf{E}\delta\boldsymbol{\varepsilon} \tag{17}$$

where an error transformation matrix $\mathbf{E}$ and an error source vector $\delta\boldsymbol{\varepsilon}$ are defined as

$$\mathbf{E} = [\mathbf{J} \quad \mathbf{JM} \quad \mathbf{JN}_1 \quad \mathbf{JN}_2] \in \Re^{6\times 48} \tag{18}$$

$$\delta\boldsymbol{\varepsilon} = \left[\delta\boldsymbol{\Lambda}^T \quad \delta\mathbf{L}^T \quad \delta\mathbf{CB}_i'^T \quad (\delta\mathbf{OA}_0 + \delta\mathbf{A})^T\right]^T \in \Re^{48\times 1} \tag{19}$$

Eq.(17) shows that all error sources are transformed to the platform errors through the error matrix.

4. Performance Measure of Accuracy

This section discusses transformation properties of the error transformation matrix $\mathbf{E}$ that transforms the structural error vector $\delta\boldsymbol{\varepsilon}$ to the platform error vector $\delta\mathbf{X}$. Based on this discussion, we will deduce an accuracy performance measure for optimum architecture design.

Consider a general transformation

$$\mathbf{y} = \mathbf{A}\mathbf{x} \tag{20}$$

where $\mathbf{x}$ and $\mathbf{y}$ are $n\times 1$ input and $m\times 1$ output vectors, respectively, and $\mathbf{A}$ is a $m\times n$ transformation matrix. To investigate how $\mathbf{A}$ affects the magnitude relationship between $\mathbf{x}$ and $\mathbf{y}$, assume that $\mathbf{x}$ lies inside a unit sphere such that

$$\|\mathbf{x}\|^2 \le 1 \tag{21}$$

then the transformed $\mathbf{x}$ lies inside an ellipsoid defined by

$$\left\|\mathbf{A}^{+}\mathbf{y}\right\|^{2} \le 1 \tag{22}$$

where $\mathbf{A}^{+}$ is a pseudoinverse of $\mathbf{A}$. The matrix $\mathbf{A}$ can be decomposed into three matrices as

$$\mathbf{A} = \mathbf{U}\Sigma\mathbf{V}^{T} \tag{23}$$

where $\mathbf{U}=[\mathbf{u}_1 \ \cdots \ \mathbf{u}_m]$ and $\mathbf{V}=[\mathbf{v}_1 \ \cdots \ \mathbf{v}_n]$ are the eigenvector matrices of $\mathbf{A}\mathbf{A}^{T}$ and $\mathbf{A}^{T}\mathbf{A}$, respectively, and $\Sigma=[diag(\sigma_1,\sigma_2,\cdots,\sigma_m) \ \mathbf{0}]$ is a matrix composed of singular values of $\mathbf{A}$ ($\sigma_1 \ge \sigma_2 \ge \cdots \ge \sigma_m \ge 0$). Using Eq.(23), the pseudoinverse of $\mathbf{A}$ can be written as

$$\mathbf{A}^{+} = \mathbf{V}\Sigma^{+}\mathbf{U}^{T} \tag{24}$$

where $\Sigma^{+}=\left[diag\left(\sigma_1^{-1},\sigma_2^{-1},\cdots,\sigma_m^{-1}\right) \ \mathbf{0}\right]^{T}$ is a pseudoinverse of Σ. Inserting Eq.(24) into Eq.(22) gives

$$\begin{aligned}\left\|\mathbf{U}\Sigma^{+}\mathbf{V}^{T}\mathbf{y}\right\|^{2} &= \left(\mathbf{y}^{T}\mathbf{V}\Sigma^{+T}\mathbf{U}^{T}\right)\left(\mathbf{U}\Sigma^{+}\mathbf{V}^{T}\mathbf{y}\right) \\ &= \left(\mathbf{V}^{T}\mathbf{y}\right)^{T} diag\left(\sigma_1^{-2},\sigma_2^{-2},\cdots,\sigma_m^{-2}\right)\left(\mathbf{V}^{T}\mathbf{y}\right) \le 1\end{aligned} \tag{25}$$

Eq.(25) depicts that $\mathbf{y}$ lies inside an error ellipsoid whose principal axes are $\mathbf{v}_1\sigma_1,\cdots,\mathbf{v}_n\sigma_n$.

The volume of the error ellipsoid defined by Eq.(25) may be interpreted as a magnitude measure of the mobile platform pose error vector $\mathbf{y}$ when the magnitude of the structural error vector $\mathbf{x}$ is restricted by unity value. This argument is similar to the manipulability measure proposed by Yoshikawa[22], which is proportional to the ellipsoid volume of a Jacobian matrix. Note that Ropponen and Arai[17] applied singular value decomposition to each component of the error transformation matrix of differential error model for Stewart platform and plotted error ellipsoid. That ellipsoid showed clearly that the dominant end point errors are found in the xy-plane and the errors in z-direction are less than one fifth of those of the other directions. In this paper, instead of looking at individual error ellipsoid of each component of the error transformation matrix, similar to the concept of manipulability measure, an error amplification factor(*EAF*) is defined from the whole error transformation matrix as

$$EAF = \sqrt{\det\left(\mathbf{E}\mathbf{E}^{T}\right)} = \prod_{i=1}^{6}(\sigma_{\mathbf{E}})_i \tag{26}$$

where $(\sigma_{\mathbf{E}})_i$ is a singular value of the error transformation matrix $\mathbf{E}$. *EAF* can be considered as an amplification measure of the structural errors to the platform pose error. The smaller the *EAF*, the smaller is the pose error. Therefore, *EAF* can be considered as a criterion on accuracy for optimum design problem.

Because *EAF* is configuration dependent, a global *EAF* over the whole workspace should be used for global optimization of the accuracy. However, in practice, the manipulator's end-effector does not span the entire workspace in the actual operation because the singular configurations are very close to the workspace boundary. Therefore, a central region around a nominal pose will be enough for most of the operation and *EAF* should be averaged in the central region of the workspace[12].

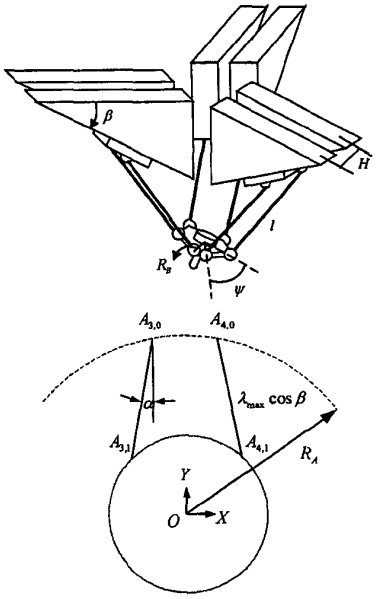

Fig. 3. Design Variables

The central region we chose is a parallelepiped whose center lies at one third, from the bottom, of the length between the upper and the lower limits of the whole workspace. In addition, for simplicity of design and analysis, the global *EAF* is averaged only at center and at each of the eight vertices of the parallelepiped workspace while the orientation of the platform is changing between the maximum and minimum orientation angles at each point. The averaged global *EAF* for accuracy criterion is then defined as

$$GEAF = \frac{\int_{V^*} EAF\,dV^*}{V^*} \tag{27}$$

where V^* is the volume of the chosen central region.

5. Formulation of the Optimization Problem

In this section, an optimization problem is formulated for the most accurate architecture design. The goal of this problem is to design a manipulator architecture that reveals minimum pose error in the platform for given structural errors. Therefore, *GEAF* is selected as a cost function to be minimized. Regarding constraints, we included desired workspace constraint, avoidance of architecture singularity,

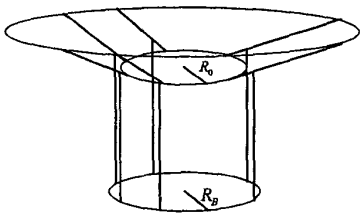

Fig. 4. Architecture Singularity of HSM

and limits in design variables.

To completely determine the HSM geometry, sixty design variables should be determined. In order to simplify the design problem, however, we reduced the number of the design variables by exploiting the symmetricity of the manipulator. Fig. 3 shows the reduced set of design variables where R_A and R_B are the radii of the circles passing through $A_{i,0}$ points and B_i points, H is the distance between the neighbor A_i points, α and β are alignment angles of the prismatic actuator, λ_{max} is a maximum actuation length from $A_{i,0}$, l is a link length, and ψ is a angle between adjacent B_i points. These eight design parameters can completely define the geometry of the HSM. However, R_A and λ_{max} are predetermined in our design process by designers for overall workspace requirements.

Singular architectures should be avoided in the design stage because an architecture singularity cannot be avoided by trajectory planning or control. Frequently met singularity in parallel mechanisms occurs when the base or the mobile platform are perpendicular to the links. In the HSM, if the radius R_0 of the circle passing through $A_{i,1}$ is smaller than radius R_B of the moving platform, an architecture singularity can occur in the vicinity of the central workspace as shown in the Fig. 4. Therefore, we included a constraint, $R_0 \geq R_B$ in the constraint set.

Mechanical collision of the HSM's structures can be avoided by restricting range of the design variables; Adjacent $A_{i,0}$ and $A_{i,1}$ points should be apart by the width of the prismatic actuators, the actuators and the links should not interfere with each other, adjacent B_i points should be apart by the amount of the spherical joint's width. The optimization problem can then be written as

$$\begin{aligned} &\textit{Minimize} && GEAF \\ &\textit{subject to} && \text{Sigularity constraint} \\ &&& \text{Design variables limits} \end{aligned} \qquad (28)$$

The *fmincon* function in MATLAB 5.2 was used to solve the optimization problem. This minimization function uses a Sequential Quadratic Programming (SQP) method, where a Quadratic Programming (QP) subproblem is solved at each iteration. An estimate of the Hessian of the Lagrangian is updated at each iteration using the BFGS formula[23].

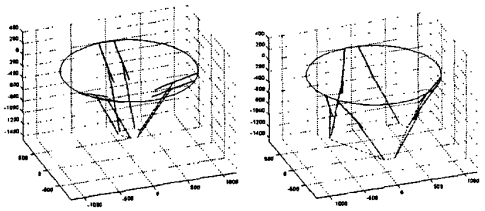

(a) Initial (b) Optimum

Fig. 5. Initial and Optimum Architectures

TABLE 1
INITIAL AND OPTIMUM VALUES

	Initial	Optimum
GEAF	0.7287×10^{-5}	0.3659×10^{-7}
H	220.0 mm	188.9mm
β	30.00°	56.40°
ψ	83.60°	105.6°
l	992.8 mm	927.9mm
R_B	165.0 mm	630.1mm
α	0°	26.88°

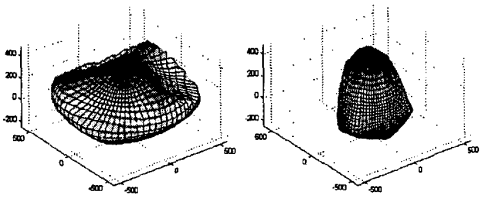

(a) Initial (b) Optimum

Fig. 6. Initial and Optimum Workspace

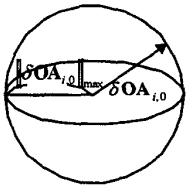

Fig. 7. Location Error Sphere

6. Optimization Results

Fig. 5 shows the initial and the optimized design of the HSM, while Table 1 shows the numerical values of the design parameters and the *GEAF*. The corresponding workspaces are shown in Fig. 6.

TABLE 2
MAXIMUM ERROR BUDGET (μm)

$\lvert\delta\lambda\rvert_{max}$	$\lvert\delta l\rvert_{max}$	$\lVert\delta\mathbf{CB}'\rVert_{max}$	$\lVert\delta\mathbf{OA}_0\rVert_{max}$	$\lVert\lambda_i\delta\mathbf{a}\rVert_{max}$
1	10	10	10	10

TABLE 3
ACCURACY COMPARISON

	Initial	Optimum
δx (mm)	52.470×10^{-3}	29.449×10^{-3}
δy (mm)	51.650×10^{-3}	27.190×10^{-3}
δz (mm)	14.328×10^{-3}	11.838×10^{-3}
$\delta\theta_x$ (°)	7.3796×10^{-3}	1.4893×10^{-3}
$\delta\theta_x$ (°)	8.9670×10^{-3}	1.3926×10^{-3}
$\delta\theta_z$ (°)	12.936×10^{-3}	1.9005×10^{-3}

In order to estimate how much the pose error of the platform is reduced by the proposed optimization method, the manipulator's accuracy has been evaluated by the Monte Carlo statistical experiment approach[21]. In the Monte Carlo simulation, for $\delta\mathbf{CB}'$, $\delta\mathbf{OA}_0$, $\delta\mathbf{A}$, we generated random vectors with uniform distribution error inside a sphere with the center at the nominal location of a point and with a radius that is the maximum allowable installation error, say 10μm radius (See Fig. 7). For $\delta\mathbf{\Lambda}$ and $\delta\mathbf{L}$, we assumed a steady state control error and a link manufacturing tolerance. All of these length errors are assumed to follow uniform distribution with maximum limits specified by an error budget guide in Table 2.
The resultant pose errors are determined by the error model in Eq.(17). The average pose error over the central parallelepiped workspace is obtained at the points where the objective function was averaged. This process is repeated 5000 times for meaningful Monte Carlo simulation[21]. We selected three times of standard deviation of the maximum pose error. Table 3 shows the simulated maximum pose error results for the initial and the optimized design. It has been shown that position errors in the X and Y direction have been reduced by approximately 40%.

7. Conclusion

In this paper, an optimal accuracy design had been performed for the HexaSlide manipulator. The possible structural errors were identified and the pose error of the platform was obtained from the error sources through the error matrix. Then using the error equation, the *EAF* that represents the error amplification factor was introduced and an accuracy criterion was defined. A design optimization of the HSM had been performed minimizing the error amplification and considering the workspace, architecture singularity, and design variable limits. Finally the pose error was evaluated by Monte Carlo simulation technique and it was shown that the optimized manipulator had smaller errors compared with the initial design.

References

[1] C. Gosselin, J. Angeles, "The Optimum Kinematic Design of a Spherical Three-degree-of-Freedom Parallel Manipulator", *ASME Trans. J. Mech., Transmissions., automat. Design*, Vol. 110, No. 2, pp. 202-207, 1989

[2] C. Gosselin, J. Angeles, "A Global Performance Index for the Kinematic Optimization of Robotic Manipulators", *ASME Trans. J. Mech Design*, Vol. 113, No. 3, pp. 220-226, 1991

[3] R. Kurtz, V. Hayward, "Multiple-Goal Kinematic Optimization of a Parallel Spherical Mechanism with Actuator Redundancy", *IEEE Trans. Robotics Automat.*, Vol. 8, No. 5, pp. 644-651, 1992

[4] O. Ma, J. Angeles, "Optimum Architecture Design of Platform Manipulator", *ICAR*, pp. 1131-1135, June, 1991

[5] K. H. Pittens, R. P. Podhorodeski, "A Family of Stewart Platforms with Optimal Dexterity", *J. Robotic Sys.*, 10(4):463-479, June, 1993

[6] K. E. Zanganeh, J. Angeles, "Kinematic Isotropy and the Optimum Design of Parallel Manipulators", *Int. J. Robotics Res.*, Vol. 16, No. 2, pp. 185-197, 1997

[7] J.-P. Merlet, "Designing a Parallel Manipulator for a Specific Workspace", *Int. J. Robotics Res.*, Vol. 16, No. 4, pp. 545-556, 1997

[8] R. Boudreau, C. M. Gosselin, "The Systhesis of Planar Parallel Manipulators with a Genetic Algorithm", *J. Mech. Design.*, Vol. 121, No. 4, pp. 533-537, 1999

[9] X. J. Liu, J. S. Wang, F. Gao, "On the Optimum Design of Planar 3-dof Parallel Manipulators with respect to the Oorkspace", *Proc. IEEE int. Conf. on Robotics Automat.*. pp. 4122-4127, 2000

[10] M. Ceccarelli, E. Ottaviano, "An Analytical Design for CAPAMAN with Prescribed Position and Orientation", *Proc. DETC*, pp. 1-8, Baltimore, Maryland, Sept, 10-13, 2000

[11] J. Schönherr, "Evaluation and Optimum Design of Parallel Manipulators having Defined Workspace", *Proc. DECTC*, pp. 1-9, Baltimore, Maryland, Sept, 10-13, 2000

[12] R. S. Stoughton, T. Arai, "A Modified Stewart Platform Manipulator with improved Dexterity", *IEEE Trans. Robotics Automat.*, Vol. 9, No. 1, pp. 166-173, 1993

[13] A. Tremblay, L. Baron, "Geometrical Synthesis of Star-Like Topology Parallel Manipulators with a Genetic Algorithm", *Proc. IEEE Int. Conf. on Robotics Automat.*, pp. 2446-2451, 1999

[14] X. J. Liu, Z. L. Jin, F. Gao, "Optimum Design of 3-dof Spherical Parallel Manipulators with respect to the Conditioning and Stiffness indices", *Mech. Mach. Theory*, Vol. 35, No. 9, pp. 1257-1267, 2000

[15] K-S Hong and J-G Kim, "Manipulability Analysis of a Parallel Machine Tool: Application to Optimal Link Length Design", *J. Robotic. Sys.*, Vol. 17, No. 8, pp. 403-415, 2000

[16] J. Wang , O. Masory, "On the Accuracy of a Stewart Platform – Part I The Effect of Manufacturing Tolerances", *Proc. IEEE Int. Conf. on Robotics Automat.*, pp. 114-120, 1993.

[17] T. Ropponen, T. Arai, "Accuracy Analysis of Modified Stewart Platform Manipulator", *Proc.1995 IEEE Int. Conf. Robotics Automat.*, 1:521-525, 1995

[18] A. J. Patel, K. F. Ehmann, "Volumetric Error of a Stewart Platform-based Machine Tool", *Annals CIRP*, Vol. 46, pp. 287-290, 1997

[19] S. Bi, G. Zong, R. Liu, S. Wang, "Accuracy Analysis of the Serial-Parallel Micromotion Manipulator", *1997 IEEE Int. Conf. Computational Cybernetics and Simulation*, Vol. 3, pp. 2258-2263

[20] F. Xi, C. Mechefske, "Modeling and Analysis of Errors in Hexapods with Fixed-Leg Lengths", *PKM 2000 Conf.*, pp. 236-244, U. of Michigan, Sept, 14-15, 2000

[21] Z. J. Pasek, "Statistical Approach to PKM Accuracy Analysis", *PKM 2000 Conf.*, pp. 42-49, U. of Michigan, Sept, 14-15, 2000

[22] T. Yoshikawa, "Manipulability of Robotic Mechanisms" *Int. J. Robotics Res.*, Vol. 4, No. 2, pp. 3-9, 1985

[23] MATLAB Optimization Toolbox User's Guide Version 2